IEEE Access
Multidisciplinary ⋮ Rapid Review ⋮ Open Access Journal

Received 19 September 2023, accepted 16 October 2023, date of publication 19 October 2023, date of current version 26 October 2023.

Digital Object Identifier 10.1109/ACCESS.2023.3325909

RESEARCH ARTICLE

Time-Periodic Metallic Metamaterials Defined by Floquet Circuits

SALVADOR MORENO-RODRÍGUEZ[1], ANTONIO ALEX-AMOR[2], PABLO PADILLA[1], JUAN F. VALENZUELA-VALDÉS[1], AND CARLOS MOLERO[1], (Member, IEEE)

[1]Department of Signal Theory, Telematics and Communications, Research Centre for Information and Communication Technologies (CITIC-UGR), University of Granada, 18071 Granada, Spain
[2]Department of Information Technology, Universidad CEU San Pablo, 28003 Madrid, Spain

Corresponding author: Salvador Moreno-Rodríguez (salvamr96@ugr.es)

This work has been supported by grant IJC2020-043599 /AEI/10.13039/501100011033 and by the European Union NextGenerationEU/PRTR. It has also been supported by grants TED2021-129938B-I00, PDC2022-133900-I00, PID2020-112545RB-C54 and TED2021-131699B-I00.

ABSTRACT In this paper, we study the scattering and diffraction phenomena in time-modulated metamaterials of metallic nature by means of Floquet equivalent circuits. Concretely, we focus on a time-periodic screen that alternates between ''metal'' and ''air'' states. We generalize our previous approaches by introducing the concepts of ''macroperiod'' and ''duty cycle'' to the time modulation. This allows to analyze time-periodic metallic metamaterials whose modulation ratios are, in general, rational numbers. Furthermore, with the introduction of the duty cycle, perfect temporal symmetry is broken within the time modulation as the time screen could remain a different amount of time in metal and air states. Previous statements lead to an enrichment of the diffraction phenomenon and to additional degrees of freedom that can be exploited in engineering to control the reflection and transmission of electromagnetic waves. Finally, we present some analytical results that are validated with a self-implemented finite-difference time-domain (FDTD) approach. Results show that the scattering level and diffraction modes can be controlled independently by means of the duty cycle and the modulation ratio, respectively, leading to an efficient design of time-based pulsed sources and beamformers.

INDEX TERMS Floquet circuit, FDTD, modulation ratio, macroperiod, duty cycle.

I. INTRODUCTION

The resolution of electromagnetic problems based on periodic structures has classically benefited from systematic simplifications thanks to the use of Floquet's theorem [1], [2]. That is, the reduction of the complexity of the whole structure to a waveguide problem [3]. Circuit models have proven to be very efficient tools to emulate waveguide environments [4], [5], [6]. Simple models avoid the *dynamic* behavior of the structure, combining transmission lines and quasi-static elements [7]. More sophisticated proposals include the contribution of higher-order modes/harmonics [8], [9], [10]. This implies the validity of the models for scenarios where higher-order harmonics have a leading role [11]. This scenario is, for instance, quite common in time-varying systems, or in a more general context, in spacetime structures [12].

Spacetime systems introduce time, generally in the form of a periodic modulation, adding non-linearities that are widely used in RF systems such as frequency dividers [13] and modulators [14]. Time implies an additional degree of freedom [15], [16], [17], [18], [19]. Though pioneering studies were theoretically reported in the middle of last century [20], [21], [22], they have regained interest in the recent years, especially when non-reciprocity [23], [24], [25] was sought as a substitute of magnetic materials for insulators [26]. Some other impressive properties have since then been reported, as temporal mechanisms for amplification [27], subharmonic mixing [28], giant bianosotropy [29], negative refraction [30], metamirrors [31] or an equivalent of the Brewster angle [32].

The associate editor coordinating the review of this manuscript and approving it for publication was Ladislau Matekovits.

Interesting applications, just to name a few, are proposed in the propagation domain focused on DOA estimation [33], imaging [34], digital processing [35].

Transmission-line and ABCD-parameter models have already been employed in electromagnetic systems with instantaneous temporal interfaces [36], [37]. Such are the cases reported in [38] and [39] and more recently in [40]. The equivalent circuit aids for a better understanding of the situations there described. However, in most cases, no periodic modulation exists and there is no excitation of higher-order harmonics. The work in [41] considers a system formed by a metallic screen suffering a periodic modulation. The system is fed by an external plane wave, exciting an infinite number of periodic Floquet harmonics. The paper reports the derivation of the circuit model but no many situations are evaluated. The present work is intended to exploit the model possibilities, increasing the number of modulation ratios, introducing the concepts of *macroperiod* and *duty cycle* to the time modulation, with the objective of enriching the diffraction phenomenon. Furthermore, it has been shown that breaking the temporal symmetry allows the suppression of non-desired harmonics [42]. The scattering parameters are quantitatively evaluated, constituting an additional contribution with respect previous works in the literature. It is worth remarking that, though the paper intention is to describe a temporal system from the theoretical point of view, the experimental time-varying scenario could be motivated by switching metasurfaces as those previously reported [43], [44], [45], [46], [47], [48], [49], [50]. Our particular case would demand a specific metasurface with periodic modulation alternating fully-transparent and fully-reflecting states.

The paper is organized as follows: Section II is left for the exposition of the time-varying scenario, explanation of the variables involved and their implications on diffraction phenomenon. Section III focuses on applying this method for reconfigurability of the propagation of electromagnetic waves. The conclusions of the work are found at the end of the paper.

II. THEORETICAL ANALYSIS

The structure under consideration is sketched in Fig. 1. A monochromatic plane wave of frequency ω_0 illuminates a time metamaterial that periodically alternates between "air" and "metal" (perfect electric conductor, PEC) states, as represented in Fig. 1(a). This can be realized by alternating two resonant states of the metamaterial, invoking fully transparency or fully reflectivity via tunable biased diodes, as can be read in [47]. Future alternatives coming from electronic materials such as graphene [51] or Vanadium oxide [52] could be promising for this purpose.

The time screen is considered to be infinitesimally thin along the propagation direction (z axis) and very large in x and y directions [see Fig. 1(b)]. Transverse magnetic, TM (E_x, E_z, H_y), or transverse electric, TE (E_y, H_x, H_z), polarizations for the oblique-incident waves are considered.

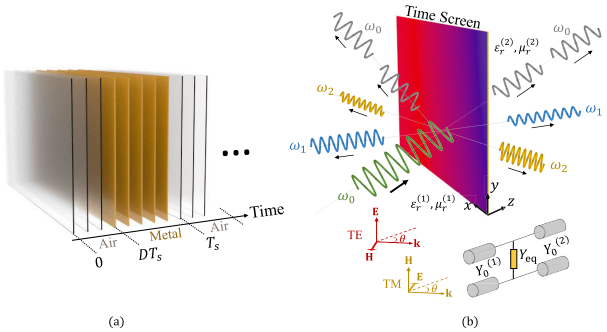

FIGURE 1. (a) Time evolution of the proposed configuration. The screen periodically alternates between "air" and "metal" states. (b) Illustration of the spacetime diffraction caused by the time-periodic screen and its equivalent circuit for both TE and TM incidence.

The time periodicity of the varying screen is $T_s = 2\pi/\omega_s$, from which the whole cycle repeats. In the more general scenario, the time screen could remain in air state (DT_s) for a different time than it remains in metal state ($[1 - D]T_s$). Here, $D \in [0, 1]$ is the *duty cycle* of the time modulation. Extreme cases $D = 0$ and $D = 1$ would imply that the time screen remains invariant in metal and air states the whole time, respectively. The fact of varying the duty cycle D and its implications were not discussed in our previous work [41], since a fixed value of $D = 0.5$ was implicitly assumed. As it will be detailed later, modifying the duty cycle enriches the diffraction phenomenon, since half-period temporal symmetry is broken and this leads to asymmetries in harmonic excitation. The *modulation ratio* $F = \omega_0/\omega_s = T_s/T_0$ constitutes a second factor to be discussed. The nature of the reflected and transmitted fields across the discontinuity directly depends on this parameter, and as it will be discussed below, it may govern the power transfer between different harmonics.

The time-periodic tangential fields are expanded in terms of Floquet-Bloch series:

$$E_t^{(1)}(x,z,t) = e^{-jk_t x}\left[e^{j\omega_0 t - j\beta_0^{(1)} z} + Re^{j\omega_0 t + j\beta_0^{(1)} z} + \sum_{\forall n\neq 0} E_n^{(1)} e^{j\omega_n t + j\beta_n^{(1)} z}\right] \quad (1)$$

$$H_t^{(1)}(x,z,t) = e^{-jk_t x}\left[Y_0^{(1)} e^{j\omega_0 t - j\beta_0^{(1)} z} - RY_0^{(1)} e^{j\omega_0 t + j\beta_0^{(1)} z} - \sum_{\forall n\neq 0} Y_n^{(1)} E_n^{(1)} e^{j\omega_n t + j\beta_n^{(1)} z}\right] \quad (2)$$

$$E_t^{(2)}(x,z,t) = e^{-jk_t x}\left[Te^{j\omega_0 t - j\beta_0^{(2)} z} + \sum_{\forall n\neq 0} E_n^{(2)} e^{j\omega_n t - j\beta_n^{(2)} z}\right] \quad (3)$$

$$H_t^{(2)}(x,z,t) = e^{-jk_t x}\left[TY_0^{(2)} e^{j\omega_0 t - j\beta_0^{(2)} z} + \sum_{\forall n\neq 0} Y_n^{(2)} E_n^{(2)} e^{j\omega_n t - j\beta_n^{(2)} z}\right] \quad (4)$$

where k_t is the transverse component of the wavevector, β_n ($n \in \mathbb{Z}$) is the nth-order longitudinal component of the wavevector associated with a nth-order harmonic, and $\omega_n = \omega_0 + n2\pi/T_m$ is the angular frequency associated to the n-th Floquet harmonic. For the sake of simplicity, the amplitude of the electric field associated with the incident wave is unity (harmonic of order $n = 0$) and its contribution is out from the summation in (1)-(4). The admittance values Y_n are expressed as

$$Y_n^{(i)} = \frac{\varepsilon_r^{(i)} \varepsilon_0 \, \omega_n}{\beta_n^{(i)}} \qquad \text{TM admittances} \tag{5}$$

$$Y_n^{(i)} = \frac{\beta_n^{(i)}}{\mu_r^{(i)} \mu_0 \, \omega_n} \qquad \text{TE admittances} \tag{6}$$

where the use of TE/TM admittances depends on the polarization of the incident wave, and $i = 1, 2$ accounts for the input and output media, respectively. It is worth remarking that the fields expanded in (1)-(4) are vectors. The vector notation have been removed for simplicity. For TM incidence the electric fields in (1) and (3) are directed along x whereas the magnetic fields in (2) and (4) points towards y. For TE incidence, the fields directions are exactly the opposite.

The higher-order Floquet coefficients $E_n^{(1/2)}$ and the reflection (R)/transmission (T) terms related to the fundamental harmonic are extracted by applying integral-equation methods on a field profile $\mathbf{E}(x, t)$ that models the dynamical behavior of the time-periodic metallic metamaterial. This methodology was previously employed in [53] and [54]. The propagation of the incident and reflected waves, and the transmitted one are represented by transmission lines with $Y_0^{(1)}$ and $Y_0^{(2)}$ characteristic admittances, respectively. In general, Floquet coefficients E_n are computed as

$$E_n^{(1)} = E_n^{(2)} = (1 + R)N(\omega_n). \tag{7}$$

The coupling between harmonics, described in terms of transformers with turn ratio $N(\omega_n)$ [see eq. (8)], demands a previous knowledge of the field profile at the discontinuity along a time period.

$$N(\omega_n) = \frac{\displaystyle\int_0^{T_m} E(x, t) e^{-j\omega_n t} dt}{\displaystyle\int_0^{T_m} E(x, t) e^{-j\omega_0 t} dt} \tag{8}$$

When the time interface is in air state, the metallic metamaterial "appears to vanish", so $\mathbf{E}(x, t)$ follows the sinusoidal shape of the incident plane wave. When the time interface is in metal state, the tangential field profile $\mathbf{E}(x, t)$ is assumed to be zero.

Moreover, R and T, can directly be estimated from the circuit model as

$$R = \frac{Y_0^{(1)} - Y_0^{(2)} - Y_{eq}}{Y_0^{(1)} + Y_0^{(2)} + Y_{eq}}, \tag{9}$$

$$T = 1 + R. \tag{10}$$

where the equivalent admittance Y_{eq} accounts for the effect of the *time discontinuity*, including the effect of all the higher-order harmonics E_n.

The equivalent admittance that models the time-periodic screen is computed as

$$Y_{eq} = \sum_{\forall n \neq 0} |N(\omega_n)|^2 (Y_n^{(1)} + Y_n^{(2)}) \tag{11}$$

Close inspection of (11) reveals that Y_{eq} is actually formed by parallel-connected transmission lines loaded with complex transformers, one for each Floquet harmonic. This allows us to expand the simplified equivalent circuit illustrated in Fig. 1(b) into the more complex, but also more physically insightful, version shown in [41]. In that sense, the admittance of the present temporal problem shares some similarities with the admittance extracted in purely spatial structures [6]. However, as discussed in our previous work [41], there also exist major differences between them. The most significant one is the fact that higher-order harmonics are propagative (of resistive nature) in the time-periodic problem while these are evanescent (of capacitive/inductive nature) in the purely spatial counterparts. Higher-order harmonics in mixed space-time scenarios are expected to contribute with both resistive and capacitive/inductive terms to the equivalent circuit.

A. MACROPERIODS

Our previous work is focused on integer time-modulation ratios F, assuming $\omega_s \leq \omega_0$ in most cases. This is a very restricted situation. The extension from integer to rational (not irrational) modulation ratios is here taken into account, modifying the way to get $\mathbf{E}(x, t)$. Now, $\mathbf{E}(x, t)$ is influenced by D and F, leading to the definition of the term *macroperiod*. A macroperiod T_m is defined as the minimum time periodicity where both the incident-wave vibration (ω_0) and the screen variation (ω_s) complete a full cycle simultaneously. Mathematically, every *rational* modulation ratio F can be approximated by a fraction of two integers, F_N and F_D, according to $F = F_N/F_D$. Since F was previously defined as $F = T_s/T_0$, the temporal macroperiod T_m must follow the condition

$$T_m = F_N T_0 = F_D T_s. \tag{12}$$

Thus, a macroperiod is completed after F_N and F_D cycles for the incident wave (T_0) and the time modulation (T_s), respectively. Please note that an *irrational* modulation ratio F cannot be described in terms of a fraction of two integers, leading to an infinite set of decimals. As a consequence, the macroperiod of an irrational modulation ratio would be infinite and the formulation proposed here would not be applicable since time periodicity is lost. Thus, the field profile is therefore defined along a macroperiod, ensuring a stationary situation. It can be mathematically described as

$$\mathbf{E}(x, t) = A(x) \sin(\omega_0 t) \, P(t) \, \hat{\mathbf{y}}, \quad t \in [0, T_m], \tag{13}$$

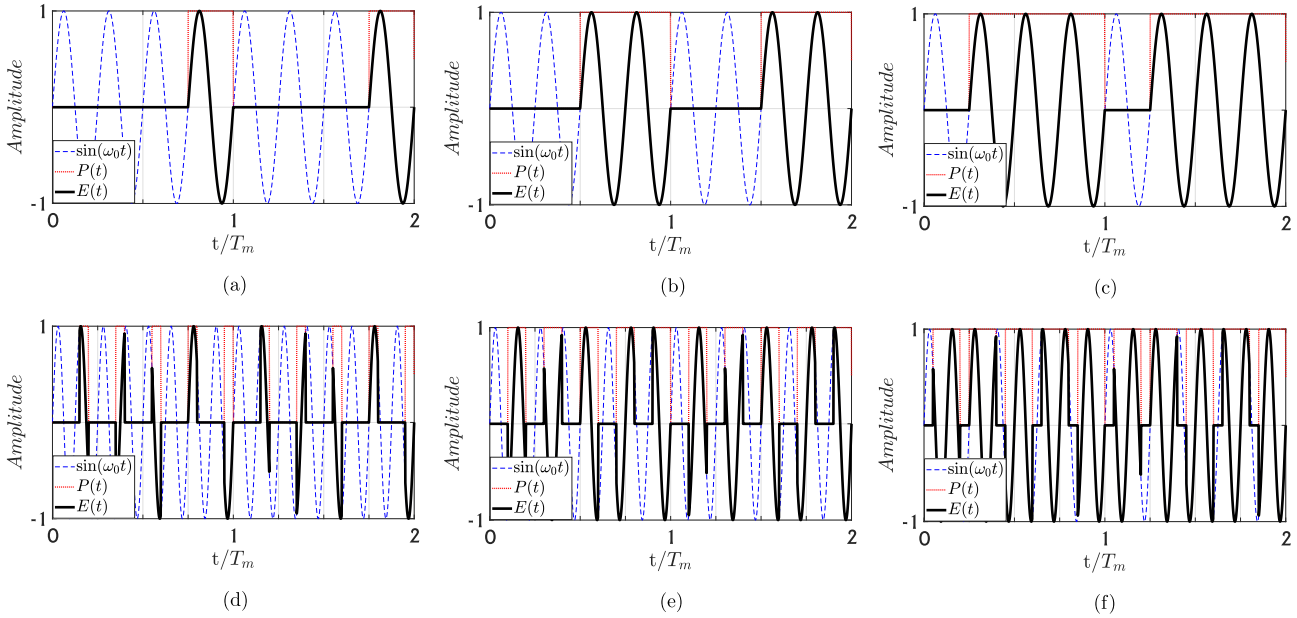

FIGURE 2. Two macroperiods of $E(t)$ when: (a) $F = 4$, $D = 0.25$, (b) $F = 4$, $D = 0.5$, (c) $F = 4$, $D = 0.75$, (d) $F = 1.6$, $D = 0.25$, (e) $F = 1.6$, $D = 0.5$, (f) $F = 1.6$, $D = 0.75$. A monochromatic incident wave of $\omega_0 = 2\pi \cdot 30$ GHz is assumed.

where $P(t)$ is a pulse train of period T_s, unit amplitude and duty cycle D, and $A(x)$ a function including the spatial dependence.

It is worth remarking that the pulse train invokes *instantaneous* switching between air/metal. Of course this is ideal. In practice this switching is not instantaneous, there exist a small (or not so small) transient time between both states. Experimental prototypes to come must neglect transient effects as much as possible. Possible solutions are based on metasurfaces with pin-diodes incorporated in the cells [55]. In addition, the frequency associated with the time-varying screen ω_s may sometimes be much slower than ω_0 (orders of few MHz Vs GHz), thus transient times, of the order of few *ns* can directly be neglected. Such is the case reported, for instance, in [35] and [43].

For the sake of simplicity, the incident wave considered in the following results has $\omega_0 = 2 \cdot \pi \cdot 30$ GHz, corresponding to a wavelenght of 10 mm. The same conclusions can be extracted at any other frequency as long as F and D remain identical. Figs. 2(a)-(c) depict the evolution of $E(t) = |\mathbf{E}(0, t)|$, when the modulation ratio is fixed to $F = 4$ ($F = F_N/F_D = 4/1$), for duty cycles $D = 0.25, 0.5, 0.75$, respectively. Notice that, given the homogeneity of the discontinuity along x, identical conclusions would be inferred when the field is evaluated at $x \neq 0$, $E(t) = E(x \neq 0, t)$. Thus $x = 0$ have been chosen for the sake of simplicity. In addition, all the field profiles $E(t)$ represented in Figs. 2 have been normalized to unity. In these cases, the value of the *macroperiod* T_m coincides with T_s (or $4T_0$). A second case regarding F as a rational number is exhibited in Figs. 2(d)-(f), where it can be appreciated how the shape of $E(t)$ becomes more complex. Now $F = 1.6 = 8/5$, increasing the macroperiod up to $T_m = 5T_s$ or, analogously, $T_m = 8T_0$. In all these figures $E(t)$ is drawn in a time interval defined by two consecutive macroperiods, in order to appreciate the existing periodicity. As will be explained below, the variation of D has direct implications on the amplitude provided by each Floquet harmonic.

B. DUTY CYCLES

A correct definition of $E(t)$ is crucial to guarantee accurate predictions by the circuit model. A first test of the validity of the circuit approach is shown in Fig. 3. It illustrates the normalized spectral response of the transmitted field in the cases reported in Fig. 2, with an inset showing the field profile $E(t)$. A TM-polarized plane wave impinging normally has been assumed for the computation. As expected, the spectrum is split in discrete harmonics, whose amplitudes vary for each case. Together with the results provided by the equivalent circuit, numerical results extracted by self-implemented finite-different time-domain (FDTD) are included. FDTD methods [56], [57] have proven to be interesting numerical alternatives to validate analytical results due to the absence of specific commercial electromagnetic solvers oriented to deal with spacetime metamaterials. It is also worthy to emphasise that due to assumption of normal incidence, all the harmonics are propagative (there is no harmonics with evanescent nature) and moreover, they leave the air-metal interface at the incidence direction ($\theta_n = 0^o$). This result comes from Eq. [28] in [41]

$$\theta_n^{(i)} = \arctan\left(\frac{k_t}{\sqrt{\varepsilon_r^{(i)}\mu_r^{(i)}\left[\frac{\omega_0 + 2\pi n/T_m}{c}\right]^2 - k_t^2}}\right) \tag{14}$$

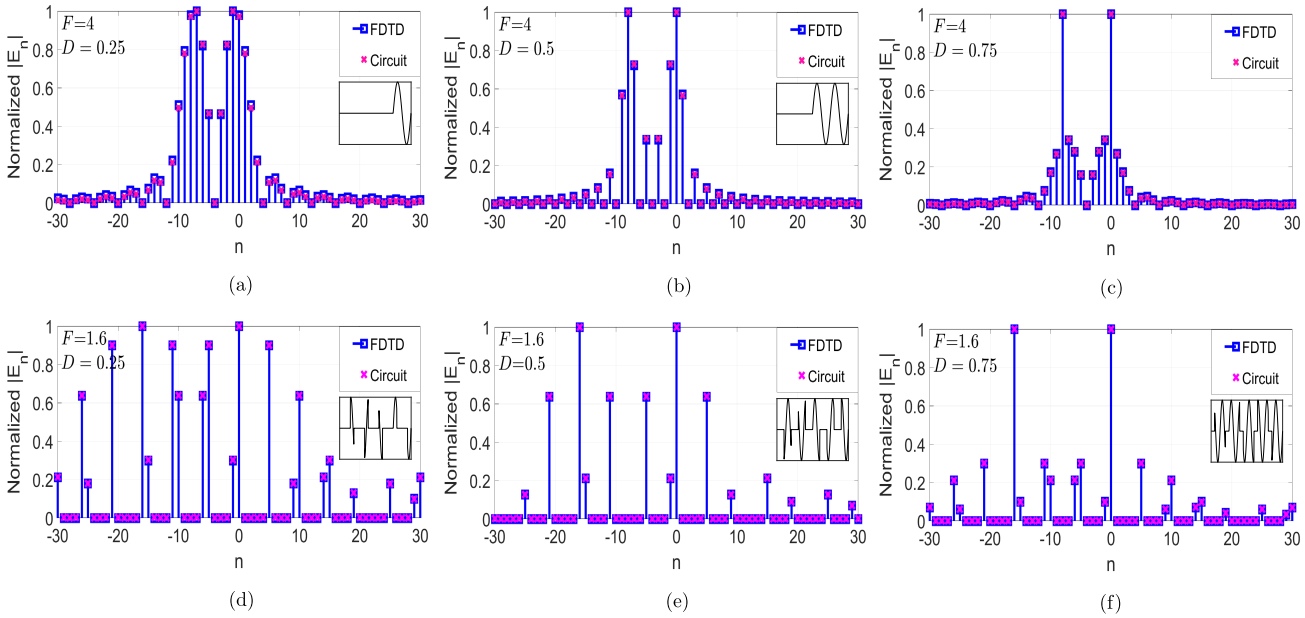

FIGURE 3. Normalized amplitude of the Floquet coefficients in the cases: (a) $F = 4$, $D = 0.25$, (b) $F = 4$, $D = 0.5$, (c) $F = 4$, $D = 0.75$, (d) $F = 1.6$, $D = 0.25$, (e) $F = 1.6$, $D = 0.5$, (f) $F = 1.6$, $D = 0.75$. A monochromatic incident wave of $\omega_0 = 2\pi \cdot 30$ GHz under normal incidence is assumed.

when imposing $k_t = 0$ with k_t being the transverse wavevector of the incident wave, and $i = 1, 2$ being the index indicating the leftmost/ rightmost medium respectively.

As visualized in Figs. 3(a)-(c) for $F = 4$, the value of D modifies the amplitude of the harmonics. For instance, when the wave encounters free-space in a longer time interval than metal at the interface, $D = 0.75$, the biggest amplitude values are carried by the fundamental harmonic ($n = 0$) and that with order $n = -8$ [see Fig. 3(c)]. When this interval decreases to $D = 0.25$, the amplitude of these predominant harmonics reduces with respect the rest of diffracted harmonics [see Fig. 3(a)]. This tendency seems to be progressive if we check Figs. 3(a)-(c) from left to right. If the modulation ratio is varied down to $F = 1.6$, as illustrated in the spectra shown in Figs. 3(d)-(f), it can be noticed that the modal distance between harmonics have changed. This fact can be appreciated since those carrying more energy are now the fundamental one ($n = 0$) and the one with order $n = -16$. In general, increasing the duty cycle D provokes that the time screen remains in "air" state a greater amount of time. Thus, the field profile $\mathbf{E}(t)$ progressively turns into the original incident plane wave as D approaches the unit. Therefore, the spectrum of the system resembles the spectrum of a conventional sine function, predominated by two delta functions at frequencies $\pm\omega_0$, with the rest of harmonics being significantly attenuated. This phenomenon is observed in Figs. 3(a)-(c) and Figs. 3(d)-(f) as D is increased. Note that breaking the perfect temporal symmetry of the modulation ($D \neq 0.5$) causes that harmonics of even and odd nature excite indistinctly. The situation was different in our previous work [41], where the duty cycle was fixed to $D = 0.5$. In that case, perfect temporal symmetry provoked that higher-order even harmonics became null, fact that can be also appreciated in Figs. 3(b) and (e). Therefore, the introduction of the duty cycle to the time modulation enriches the diffraction spectrum, which is of potential interest for the development of time-based beamformers.

III. DIFFRACTION RECONFIGURABILITY

To understand the effect of the reconfigurability in this time-periodic metamaterial, Fig. 4 shows configurations with different modulation ratios F while keeping the same duty cycle fixed to $D = 0.5$. This situation is well captured by the circuit model, after a previous definition of $E(t)$. The temporal evolution of $E(t)$ along a macroperiod is included as an inset of the figures. Now, TE oblique incidence is assumed under an angle of incidence $\theta_{\text{inc}} = 30^{\text{o}}$. The transverse wavevector is no longer null ($k_t \neq 0$), opening the possibility to excite evanescent harmonics according to (14). Fig. 4(a) depicts a first case governed by $F = 2.5$. For this configuration, some evanescent harmonics have non-zero amplitude values, as those with orders $n = -6, -4$. The rest of harmonics with non-zero amplitude are propagative. As F changes, the amplitude distribution get modified. In case illustrated in Fig. 4(b) the modulation ratio is $F = 1.6$, and now the evanescent harmonics with significant amplitude are those with orders $n = -11, -5$. For $F = 0.8$, reported in Fig. 4(c), they become the ones with orders $n = -5, -3$.

The harmonics with propagative nature appearing in Fig. 4 now scatters in different directions. The diffraction angles of each propagating harmonic have been calculated using (14). They have been compared with the angles obtained by FDTD in TABLE 1 under two different incident angles: $\theta_{inc} = 30^{\text{o}}$ and $\theta_{inc} = 50^{\text{o}}$. As observed, there is a good agreement between both analytical (Floquet circuit) and numerical results. Naturally, one point to note is

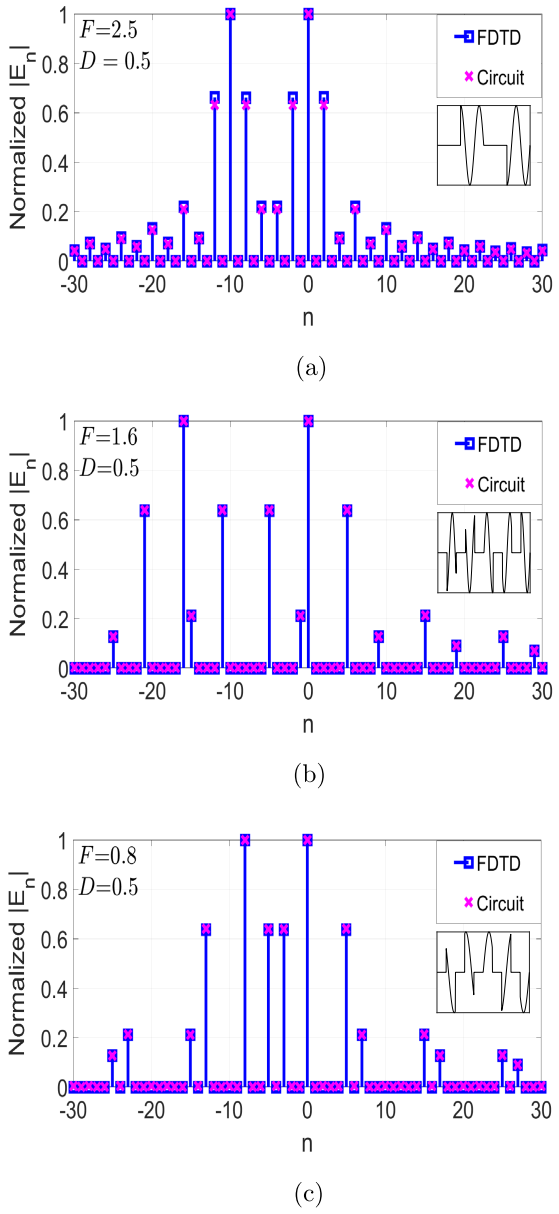

FIGURE 4. Normalized amplitude of the Floquet coefficients in the cases: (a) $F = 2.5$, $D = 0.5$, (b) $F = 1.6$, $D = 0.5$, (c) $F = 0.8$, $D = 0.5$. A monochromatic incident wave of $\omega_0 = 2\pi \cdot 30$ GHz under oblique incidence is assumed: $\theta_{inc} = 30^o$.

TABLE 1. Diffraction angle θ_n of the main Floquet harmonics for different modulation ratios F. A monochromatic incident wave with $\omega_0 = 2\pi \cdot 30 \cdot 10^9\ s^{-1}$ under oblique incidences is considered. Incidence angles: $\theta_{inc} = 30^o$ and $\theta_{inc} = 50^o$. The duty cycle of the time-periodic screen is $D = 0.5$.

	θ_{inc}	θ_n	Circuit	FDTD
$F = 2.5$	30^o	$\theta_{-2}(^o)$	56.44	56.49
		$\theta_0(^o)$	30.00	29.97
		$\theta_2(^o)$	20.92	20.93
		$\theta_4(^o)$	16.12	16.17
		$\theta_6(^o)$	13.13	13.17
	50^o	$\theta_{-2}(^o)$	eva.	eva.
		$\theta_0(^o)$	50.00	49.96
		$\theta_2(^o)$	33.17	33.18
		$\theta_4(^o)$	25.18	25.17
		$\theta_6(^o)$	20.37	20.30
$F = 1.6$	30^o	$\theta_0(^o)$	30.00	29.98
		$\theta_5(^o)$	17.92	17.95
		$\theta_9(^o)$	13.60	13.63
		$\theta_{15}(^o)$	10.01	10.03
	50^o	$\theta_0(^o)$	50.00	49.96
		$\theta_5(^o)$	28.12	28.10
		$\theta_9(^o)$	21.13	21.15
		$\theta_{15}(^o)$	15.45	15.48
$F = 0.8$	30^o	$\theta_0(^o)$	30.00	29.98
		$\theta_5(^o)$	12.83	12.87
		$\theta_7(^o)$	10.47	10.50
		$\theta_{15}(^o)$	6.04	6.02
	50^o	$\theta_0(^o)$	50.00	50.02
		$\theta_5(^o)$	19.90	19.92
		$\theta_7(^o)$	16.17	16.17
		$\theta_{15}(^o)$	9.28	9.31

the difference in simulation times for each solution. The analytical Floquet solution reduces notably the computational complexity compared to the FDTD. Concretely, the circuit model requires a simulation time of the order of seconds, while the FDTD takes minutes to simulate the scenario. This becomes more evident as the macroperiod of the time-modulated metamaterial is larger.

Subsequently, Fig. 5 illustrates the electric field distribution in the transmission region ($z > 0$) for the cases reported in TABLE 1. The simulation space takes $40\lambda_0 \times 20\lambda_0$. For simplicity, in all cases it has been assumed a fixed duty cycle of $D = 0.5$. These diffraction patterns obtained by FDTD allows for a clear identification of the direction of some harmonics. Some other harmonics taking place in the whole field expansion do not appear for the following reasons: their amplitude is not significant; they have an evanescent nature; they propagate backwards ($\beta_n^{(2)} < 0$). Thus, Fig. 5(a) and Fig. 5(d) show the diffraction pattern for a fixed modulation ratio $F = 2.5$ under the incident angles: $\theta_{inc} = 30^o$ and $\theta_{inc} = 50^o$, respectively. Please, note that the increase of the incident angle does not modify the excitation of the Floquet modes, but some of them are converted from propagative to evanescent nature. For this reason, the harmonic with order $n = -2$ does not appear when the incident angle rises up to 50^o. In Fig. 5(b) and Fig. 5(e), the modulation ratio has been fixed to $F = 1.6$. As it is expected according to Fig. 4, the index of the excited harmonics and, consequently, their frequencies are modified. As F decreases, it can be noticed that the diffraction angle of higher-order harmonics separate from that of the fundamental harmonic ($\theta_0 = 30^o$ for Fig. 5(b) and $\theta_0 = 50^o$ for Fig. 5(e)), approaching the

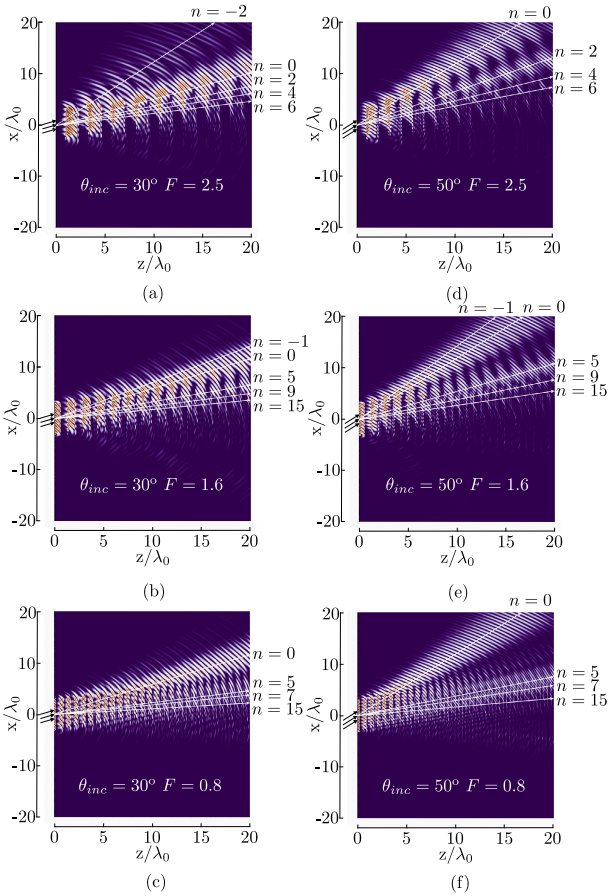

FIGURE 5. Electric field distribution obtained by means of FDTD method for the cases: (a) $F = 2.5$, $\theta_{inc} = 30^o$, (b) $F = 1.6$, $\theta_{inc} = 30^o$, (c) $F = 0.8$, $\theta_{inc} = 30^o$, (d) $F = 2.5$, $\theta_{inc} = 50^o$, (e) $F = 1.6$, $\theta_{inc} = 50^o$, (f) $F = 0.8$, $\theta_{inc} = 50^o$. Duty cycle has been fixed to $D = 0.5$ in all cases. A monochromatic incident wave of $\omega_0 = 2\pi \cdot 30$ GHz is assumed.

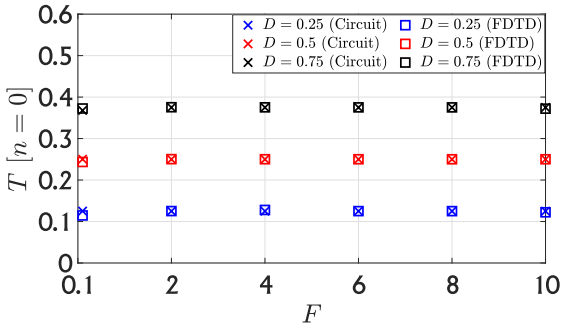

FIGURE 6. Transmission coefficient T as a function of the modulation ratio F for different duty cycles D.

normal direction ($\theta_n \approx 0^o$). This is accurately predicted by (14). This phenomenon becomes even more pronounced in Fig. 5(c) and Fig. 5(f), where the modulation ratio is $F = 0.8$. The identification of higher harmonics becomes significantly more challenging in this scenario.

Finally, Fig. 6 shows the transmission coefficient T, related to the fundamental harmonic ($n = 0$), for several values of the modulation ratio F and duty cycle D. Normal incidence is now considered, though oblique incidence can straightforwardly be computed. A comparison is illustrated between the results extracted from the Floquet circuit and the FDTD method, showing an good agreement. It can be appreciated that, for a fixed duty cycle, the transmission coefficient remains constant regardless of the value of the modulation ratio. Conversely, the transmission coefficient increases as the duty cycle does. This is due to the fact that the time-periodic screen remains a greater amount of time in the "air" state than in the "metal" state, allowing the incident waves to pass through it more easily in average.

IV. CONCLUSION

To conclude, in this Manuscript, we have studied the diffraction of electromagnetic fields produced by an incident plane wave with TE/TM polarization impinging on a time-periodic metallic screen. The proposed time-modulated metamaterial periodically alternates between "air" and "metal" states, leading to the excitation of diffraction orders that can be exploited to manipulate the propagation of electromagnetic waves. We have carried out the analysis by means of two tools: an analytical Floquet circuit and a numerical FDTD method. By introducing the concepts of "macroperiod" (T_m) and "duty cycle" (D) to the time modulation, we have extended the beamforming capabilities of the temporal structure shown in our previous works. The reconfigurability of higher-order modes has been discussed as a function of changes in the modulation ratio F and the duty cycle D. These results open up the possibility to simulate time-varying structures in a much more faster and efficient way than other full-wave electromagnetic tools, with the aim of designing modern time-based microwave and photonic devices.

REFERENCES

[1] C. Elachi, "Waves in active and passive periodic structures: A review," *Proc. IEEE*, vol. 64, no. 12, pp. 1666–1698, Dec. 1976.

[2] A. Alex-Amor, Á. Palomares-Caballero, and C. Molero, "3-D metamaterials: Trends on applied designs, computational methods and fabrication techniques," *Electronics*, vol. 11, no. 3, p. 410, Jan. 2022.

[3] J. E. Varela and J. Esteban, "Characterization of waveguides with a combination of conductor and periodic boundary contours: Application to the analysis of bi-periodic structures," *IEEE Trans. Microw. Theory Techn.*, vol. 60, no. 3, pp. 419–430, Mar. 2012.

[4] N. Marcuvitz, *Waveguide Handbook*, no. 21. IET, 1986.

[5] F. Costa, A. Monorchio, and G. Manara, "Efficient analysis of frequency-selective surfaces by a simple equivalent-circuit model," *IEEE Antennas Propag. Mag.*, vol. 54, no. 4, pp. 35–48, Aug. 2012.

[6] F. Mesa, R. Rodriguez-Berral, and F. Medina, "Unlocking complexity using the ECA: The equivalent circuit model as an efficient and physically insightful tool for microwave engineering," *IEEE Microw. Mag.*, vol. 19, no. 4, pp. 44–65, Jun. 2018.

[7] O. Luukkonen, C. Simovski, G. Granet, G. Goussetis, D. Lioubtchenko, A. V. Raisanen, and S. A. Tretyakov, "Simple and accurate analytical model of planar grids and high-impedance surfaces comprising metal strips or patches," *IEEE Trans. Antennas Propag.*, vol. 56, no. 6, pp. 1624–1632, Jun. 2008.

[8] R. Rodríguez-Berral, F. Mesa, and F. Medina, "Analytical multimodal network approach for 2-D arrays of planar patches/apertures embedded in a layered medium," *IEEE Trans. Antennas Propag.*, vol. 63, no. 5, pp. 1969–1984, May 2015.

[9] A. Alex-Amor, F. Mesa, Á. Palomares-Caballero, C. Molero, and P. Padilla, "Exploring the potential of the multi-modal equivalent circuit approach for stacks of 2-D aperture arrays," *IEEE Trans. Antennas Propag.*, vol. 69, no. 10, pp. 6453–6467, Oct. 2021.

[10] C. Molero, A. Alex-Amor, F. Mesa, Á. Palomares-Caballero, and P. Padilla, "Cross-polarization control in FSSs by means of an equivalent circuit approach," *IEEE Access*, vol. 9, pp. 99513–99525, 2021.

[11] C. Molero, R. Rodríguez-Berral, F. Mesa, F. Medina, M. Memarian, and T. Itoh, "Planar resonant blazed gratings from a circuit model standpoint," *IEEE Trans. Antennas Propag.*, vol. 68, no. 4, pp. 2765–2778, Apr. 2020.

[12] S. Taravati and G. V. Eleftheriades, "Generalized space-time-periodic diffraction gratings: Theory and applications," *Phys. Rev. Appl.*, vol. 12, Aug. 2019, Art. no. 024026, doi: 10.1103/PhysRevApplied.12.024026.

[13] H. Chen, M. Liu, A. Li, and E. H. W. Chan, "Microwave frequency dividers with reconfigurable fractional 2/N and 3/N division ratios," *IEEE Access*, vol. 11, pp. 29128–29137, 2023.

[14] S. Sugiura, T. Ishihara, and M. Nakao, "State-of-the-art design of index modulation in the space, time, and frequency domains: Benefits and fundamental limitations," *IEEE Access*, vol. 5, pp. 21774–21790, 2017.

[15] V. Pacheco-Peña, D. M. Solís, and N. Engheta, "Time-varying electromagnetic media: Opinion," *Opt. Mater. Exp.*, vol. 12, no. 10, pp. 3829–3836, Oct. 2022. [Online]. Available: https://opg.optica.org/ome/abstract.cfm?URI=ome-12-10-3829

[16] C. Caloz and Z.-L. Deck-Léger, "Spacetime metamaterials—Part I: General concepts," *IEEE Trans. Antennas Propag.*, vol. 68, no. 3, pp. 1569–1582, Mar. 2020.

[17] C. Caloz and Z.-L. Deck-Léger, "Spacetime metamaterials—Part II: Theory and applications," *IEEE Trans. Antennas Propag.*, vol. 68, no. 3, pp. 1583–1598, Mar. 2020.

[18] K. J. Deshmukh and G. W. Milton, "An energy conserving mechanism for temporal metasurfaces," *Appl. Phys. Lett.*, vol. 121, no. 4, Jul. 2022, Art. no. 041702.

[19] E. Galiffi, R. Tirole, S. Yin, H. Li, S. Vezzoli, P. A. Huidobro, M. G. Silveirinha, R. Sapienza, A. Alù, and J. B. Pendry, "Photonics of time-varying media," *Adv. Photon.*, vol. 4, no. 1, Feb. 2022, Art. no. 014002, doi: 10.1117/1.AP.4.1.014002.

[20] M. Moshinsky, "Diffraction in time," *Phys. Rev.*, vol. 88, pp. 625–631, Nov. 1952.

[21] F. R. Morgenthaler, "Velocity modulation of electromagnetic waves," *IEEE Trans. Microw. Theory Techn.*, vol. MTT-6, no. 2, pp. 167–172, Apr. 1958.

[22] T. Tamir, H. C. Wang, and A. A. Oliner, "Wave propagation in sinusoidally stratified dielectric media," *IEEE Trans. Microw. Theory Techn.*, vol. MTT-12, no. 3, pp. 323–335, May 1964.

[23] J. W. Zang, D. Correas-Serrano, J. T. S. Do, X. Liu, A. Alvarez-Melcon, and J. S. Gomez-Diaz, "Nonreciprocal wavefront engineering with time-modulated gradient metasurfaces," *Phys. Rev. Appl.*, vol. 11, no. 5, May 2019, Art. no. 054054.

[24] D. L. Sounas and A. Alù, "Non-reciprocal photonics based on time modulation," *Nature Photon.*, vol. 11, no. 12, pp. 774–783, Dec. 2017.

[25] A. Alex-Amor, C. Molero, and M. G. Silveirinha, "Analysis of metallic space-time gratings using Lorentz transformations," *Phys. Rev. Appl.*, vol. 20, no. 1, Jul. 2023, Art. no. 014063.

[26] S. Taravati, N. Chamanara, and C. Caloz, "Nonreciprocal electromagnetic scattering from a periodically space-time modulated slab and application to a quasisonic isolator," *Phys. Rev. B, Condens. Matter*, vol. 96, no. 16, Oct. 2017, Art. no. 165144. [Online]. Available: https://link.aps.org/doi/10.1103/PhysRevB.96.165144

[27] J. B. Pendry, E. Galiffi, and P. A. Huidobro, "Gain in time-dependent media—A new mechanism," *J. Opt. Soc. Amer. B, Opt. Phys.*, vol. 38, no. 11, pp. 3360–3366, Nov. 2021. [Online]. Available: https://opg.optica.org/josab/abstract.cfm?URI=josab-38-11-3360

[28] Z. Wu, C. Scarborough, and A. Grbic, "Space-time-modulated metasurfaces with spatial discretization: Free-space N-path systems," *Phys. Rev. Appl.*, vol. 14, no. 6, Dec. 2020, Art. no. 064060.

[29] P. A. Huidobro, M. G. Silveirinha, E. Galiffi, and J. B. Pendry, "Homogenization theory of space-time metamaterials," *Phys. Rev. Appl.*, vol. 16, no. 1, Jul. 2021, Art. no. 014044, doi: 10.1103/PhysRevApplied.16.014044.

[30] V. Bruno, C. DeVault, S. Vezzoli, Z. Kudyshev, T. Huq, S. Mignuzzi, A. Jacassi, S. Saha, Y. D. Shah, S. A. Maier, D. R. S. Cumming, A. Boltasseva, M. Ferrera, M. Clerici, D. Faccio, R. Sapienza, and V. M. Shalaev, "Negative refraction in time-varying strongly coupled plasmonic-antenna-epsilon-near-zero systems," *Phys. Rev. Lett.*, vol. 124, no. 4, Jan. 2020, Art. no. 043902.

[31] R. Tirole, E. Galiffi, J. Dranczewski, T. Attavar, B. Tilmann, Y.-T. Wang, P. A. Huidobro, A. Alù, J. B. Pendry, S. A. Maier, S. Vezzoli, and R. Sapienza, "Saturable time-varying mirror based on an epsilon-near-zero material," *Phys. Rev. Appl.*, vol. 18, no. 5, Nov. 2022, Art. no. 054067.

[32] V. Pacheco-Peña and N. Engheta, "Temporal equivalent of the Brewster angle," *Phys. Rev. B, Condens. Matter*, vol. 104, no. 21, Dec. 2021, Art. no. 214308, doi: 10.1103/PhysRevB.104.214308.

[33] X. Fang, M. Li, J. Han, D. Ramaccia, A. Toscano, F. Bilotti, and D. Ding, "Low-complexity DoA estimation method based on space-time modulated metasurfaces," in *Proc. IEEE Int. Symp. Antennas Propag. USNC-URSI Radio Sci. Meeting (AP-S/URSI)*, Jul. 2022, pp. 1282–1283.

[34] B. H. Kolner, "Space-time imaging, magnification, and time reversal of matter waves," *Appl. Phys. Lett.*, vol. 117, no. 12, Sep. 2020, Art. no. 124001.

[35] L. Li, H. Zhao, C. Liu, L. Li, and T. J. Cui, "Intelligent metasurfaces: Control, communication and computing," *eLight*, vol. 2, no. 1, p. 7, May 2022.

[36] Y. Xiao, D. N. Maywar, and G. P. Agrawal, "Reflection and transmission of electromagnetic waves at a temporal boundary," *Opt. Lett.*, vol. 39, no. 3, pp. 574–577, Feb. 2014. [Online]. Available: https://opg.optica.org/ol/abstract.cfm?URI=ol-39-3-574

[37] S. Y. Elnaggar and G. N. Milford, "Modeling space–time periodic structures with arbitrary unit cells using time periodic circuit theory," *IEEE Trans. Antennas Propag.*, vol. 68, no. 9, pp. 6636–6645, Sep. 2020.

[38] D. Ramaccia, A. Toscano, and F. Bilotti, "Light propagation through metamaterial temporal slabs: Reflection, refraction, and special cases," *Opt. Lett.*, vol. 45, no. 20, pp. 5836–5839, Oct. 2020. [Online]. Available: https://opg.optica.org/ol/abstract.cfm?URI=ol-45-20-5836

[39] D. Ramaccia, A. Alù, A. Toscano, and F. Bilotti, "Temporal multilayer structures for designing higher-order transfer functions using time-varying metamaterials," *Appl. Phys. Lett.*, vol. 118, no. 10, Mar. 2021, Art. no. 101901.

[40] L. Stefanini, S. Yin, D. Ramaccia, A. Alù, A. Toscano, and F. Bilotti, "Temporal interfaces by instantaneously varying boundary conditions," *Phys. Rev. B, Condens. Matter*, vol. 106, no. 9, Sep. 2022, Art. no. 094312, doi: 10.1103/PhysRevB.106.094312.

[41] A. Alex-Amor, S. Moreno-Rodríguez, P. Padilla, J. F. Valenzuela-Valdés, and C. Molero, "Diffraction phenomena in time-varying metal-based metasurfaces," *Phys. Rev. Appl.*, vol. 19, Apr. 2023, Art. no. 044014, doi: 10.1103/PhysRevApplied.19.044014.

[42] A. Gebhard, S. Sadjina, S. Tertinek, K. Dufrene, H. Pretl, and M. Huemer, "A harmonic rejection strategy for 25% duty-cycle IQ-mixers using digital-to-time converters," *IEEE Trans. Circuits Syst. II, Exp. Briefs*, vol. 67, no. 7, pp. 1229–1233, Jul. 2020.

[43] S. Taravati and G. V. Eleftheriades, "Microwave space-time-modulated metasurfaces," *ACS Photon.*, vol. 9, no. 2, pp. 305–318, Feb. 2022.

[44] Y. Liu, Y. Wang, X. Fu, L. Shi, F. Yang, J. Luo, Q. Y. Zhou, Y. Fu, Q. Chen, J. Y. Dai, L. Zhang, Q. Cheng, and T. J. Cui, "Toward sub-terahertz: Space–time coding metasurface transmitter for wideband wireless communications," *Adv. Sci.*, Aug. 2023, Art. no. 2304278, doi: 10.1002/advs.202304278.

[45] V. Kozlov, D. Vovchuk, and P. Ginzburg, "Broadband radar invisibility with time-dependent metasurfaces," *Sci. Rep.*, vol. 11, no. 1, p. 14187, Jul. 2021. [Online]. Available: https://api.semanticscholar.org/CorpusID:233324557

[46] X. Fang, M. Li, D. Ramaccia, A. Toscano, F. Bilotti, and D. Ding, "Self-adaptive retro-reflective Doppler cloak based on planar space-time modulated metasurfaces," *Appl. Phys. Lett.*, vol. 122, no. 2, Jan. 2023, Art. no. 021702, doi: 10.1063/5.0132125.

[47] L. Zhang, X. Q. Chen, S. Liu, Q. Zhang, J. Zhao, J. Y. Dai, G. D. Bai, X. Wan, Q. Cheng, G. Castaldi, V. Galdi, and T. J. Cui, "Space-time-coding digital metasurfaces," *Nature Commun.*, vol. 9, no. 1, p. 4334, Oct. 2018.

[48] J. Zhang, P. Li, R. C. C. Cheung, A. M. H. Wong, and J. Li, "Generation of time-varying orbital angular momentum beams with space-time-coding digital metasurface," *Adv. Photon.*, vol. 5, no. 3, Apr. 2023, Art. no. 036001, doi: 10.1117/1.AP.5.3.036001.

[49] Y. Zhu, X. Fang, Z. Lai, M. Li, and D. Ding, "Low complexity design methods of the space-time modulated metasurface: Theory and experiments," in *Proc. 17th Eur. Conf. Antennas Propag. (EuCAP)*, Mar. 2023, pp. 1–4.

[50] Z. Xu, X. Kong, J. Chang, D. F. Sievenpiper, and T. J. Cui, "Topological flat bands in self-complementary plasmonic metasurfaces," *Phys. Rev. Lett.*, vol. 129, no. 25, Dec. 2022, Art. no. 253001, doi: 10.1103/PhysRevLett.129.253001.

[51] C. Huang, J. Liao, C. Ji, J. Peng, L. Yuan, and X. Luo, "Graphene-integrated reconfigurable metasurface for independent manipulation of reflection magnitude and phase," *Adv. Opt. Mater.*, vol. 9, no. 7, Apr. 2021, Art. no. 2001950, doi: 10.1002/adom.202001950.

[52] C. V. S. Kumar, F. Maury, and N. Bahlawane, "Vanadium oxide as a key constituent in reconfigurable metamaterials," in *Metamaterials and Metasurfaces*. IntechOpen, 2018.

[53] R. Rodriguez-Berral, C. Molero, F. Medina, and F. Mesa, "Analytical wideband model for strip/slit gratings loaded with dielectric slabs," *IEEE Trans. Microw. Theory Techn.*, vol. 60, no. 12, pp. 3908–3918, Dec. 2012.

[54] F. Mesa, M. García-Vigueras, F. Medina, R. Rodríguez-Berral, and J. R. Mosig, "Circuit-model analysis of frequency selective surfaces with scatterers of arbitrary geometry," *IEEE Antennas Wireless Propag. Lett.*, vol. 14, pp. 135–138, 2015.

[55] (Oct. 2023). *SMP1320-Series*. [Online]. Available: https://www.skyworksinc.com/en/Products/Diodes/SMP1320-Series

[56] S. A. Stewart, Tom. J. Smy, and S. Gupta, "Finite-difference time-domain modeling of space–time-modulated metasurfaces," *IEEE Trans. Antennas Propag.*, vol. 66, no. 1, pp. 281–292, Jan. 2018.

[57] Y. Vahabzadeh, N. Chamanara, and C. Caloz, "Generalized sheet transition condition FDTD simulation of metasurface," *IEEE Trans. Antennas Propag.*, vol. 66, no. 1, pp. 271–280, Jan. 2018.

SALVADOR MORENO-RODRÍGUEZ received the B.Sc. and M.Sc. degrees in telecommunication engineering from the University of Granada (UGR), Spain, in 2019 and 2021, respectively, where he is currently pursuing the Ph.D. degree. Since 2021, he has been with the Department of Signal Theory, Telematics and Communications, Research Centre for Information and Communication Technologies (CITIC-UGR). His current research interests include polarizers, metamaterials, and applied electromagnetism.

ANTONIO ALEX-AMOR received the B.Sc. degree in telecommunication engineering from the University of Granada (UGR), Granada, Spain, in 2016, and the M.Sc. and Ph.D. degrees in telecommunication engineering from Universidad Politécnica de Madrid (UPM) in 2018 and 2021, respectively. From 2016 to 2021, he was with the Radiation Group, Department of Signal, Systems and Radiocommunications, UPM. From 2018 to 2019, he was with the Department of Language and Computer Science, Universidad de Málaga. From 2020 to 2021, he was with the Departamento de Teoría de la Señal, Telemática y Telecomunicaciones, UGR. He is currently an Assistant Professor with Universidad CEU San Pablo, Madrid, Spain. He was a Visiting Student with the KTH Royal Institute of Technology in 2019 for four months and conducted a Short Postdoctoral Mission with Universidade de Lisboa, Lisbon, Portugal, in 2021. His current research interests include the analysis and design of metamaterial structures and antennas, and wireless communication systems. In 2020, he received the Best Electromagnetics Paper Award at the 14th European Conference on Antennas and Propagation (EuCAP 2020). He is also an active science communicator in blogs and social media.

PABLO PADILLA was born in Jaén, Spain, in 1982. He received the degree in telecommunication engineering and the Ph.D. degree from the Radiation Group, Department of Signal, Systems and Radiocommunications, Technical University of Madrid (UPM), Spain, in 2005 and 2009, respectively. In 2007, he was an invited Ph.D. Student with the Laboratory of Electromagnetism and Acoustics, École Polytechnique Fédérale de Lausanne, Lausanne, Switzerland. In 2009, he carried out a postdoctoral position with the Helsinki University of Technology (AALTO, formerly TKK). In 2009, he became an Assistant Professor with the Department of Signal Theory, Telematics and Communications, University of Granada, where he has been an Associate Professor, since 2012. In 2017, he was an invited Visiting Professor with the Royal Institute of Technology of Stockholm. He has authored more than 65 high-impact journal contributions and more than 60 contributions to international symposia. His research interests include a variety of topics related mainly to electromagnetism and communication issues (radiofrequency devices, antennas, and propagation).

JUAN F. VALENZUELA-VALDÉS was born in Marbella, Spain. He received the degree in telecommunication engineering from Universidad de Málaga, Málaga, Spain, in 2003, and the Ph.D. degree from Universidad Politécnica de Cartagena, Cartagena, Spain, in 2008. In 2004, he joined the Department of Information Technologies and Communications, Universidad Politécnica de Cartagena. In 2007, he joined EMITE Ing., Murcia, Spain, as the Head of Research. In 2011, he joined Universidad de Extremadura, Mérida, Spain. In 2015, he joined Universidad de Granada, Granada, Spain, where he is currently a Full Professor, the Head of the SWAT Research Group, and the Co-Head of the Singular Laboratory of electromagnetic characterization of microwave and millimeter devices and antennas. His publication record comprised of more than 100 publications, including 50 Journal Citation Reports (JCR) indexed articles and seven book chapters. He holds several national and international patents. His current research interests include wireless communications, radio frequency devices, antennas, and propagation. He received several prizes, including the National Prize for the Best Ph.D. in mobile communications by Vodafone.

CARLOS MOLERO (Member, IEEE) was born in Seville, Spain, in April 1987. He received the Licenciado and Ph.D. degrees in physics from Universidad de Sevilla, Seville, in 2011 and 2017, respectively. From 2017 to 2020, he held a postdoctoral position with INSA Rennes, Rennes, France. Since 2020, he has been a Postdoctoral Researcher with the University of Granada. His research interests include the study of periodic structures, both in planar and 3-D architectures, circuit models, full-metal devices, a new conception of polarizers based on 3-D printable self-supported cells, and space-time metasurfaces. He was a recipient of some prizes, such as the Best Engineer Prize from the European Microwave Conference of 2015, Paris, France.